Collaborative Research: Characterization of Microwave Continuum Emission from Ultra-high Energy Cosmic Ray Extensive Air Showers

P. W. Gorham,[1] J. J. Beatty,[2] P. Miočinović,[1] and G. S. Varner[1]

[1]*University of Hawaii at Manoa, Department of Physics and Astronomy, Honolulu, Hawaii 96822*
[2]*Dept. of Physics, Ohio State University, Columbus, Ohio 43210-1117*

I. PROJECT DESCRIPTION

A. Introduction

The origin and nature of the ultra-high energy cosmic rays (UHECR) remains one of the enduring mysteries of experimental particle astrophysics. In spite of well over four decades of observations of 10^{20} eV UHECR by many different experiments [1], we still do not have a confirmed astrophysical source for these particles, nor do we understand their composition in any detail, nor do we know how they propagate from their unknown sources to earth [2]. In the last decade new observatories such as HiRes and most recently the Auger Observatory have much improved the statistics on measurements of these particles, but the issues of their origin and propagation remain largely open. As the highest energy subatomic particles observed in nature, UHECRs must arise from the most energetic phenomena in our universe. Their study is thus crucial to understanding the nature of acceleration processes that can attain energies some seven orders of magnitude higher than is currently achievable in the laboratory [3, 4, 5].

The primary UHECR spectrum is described by a simple power law $J(E) \propto E^{-\alpha}$ with $\alpha \simeq 2.7$ for $10^{18.5} < E < 10^{19.5}$ eV [6, 23]. Above $10^{19.5}$, the interaction length of cosmic ray nucleons on the cosmic microwave background becomes comparable to intergalactic separation distances, a process first described by Greisen [8], and Zatsepin & Kuzmin [9] and now known as the GZK process. It is precisely at and above the GZK energies that the measurements of the primary UHECR become uncertain due to low statistics, and the shape of the spectrum near the endpoint is still a subject of active debate.

Because of the scarcity of particles at these highest energies, research into new methods has focused on indirect means of observation [24, 25], which makes use of radiated air-fluorescence emission from the air shower to observe it at distances of up to tens of km from the particle axis. By observing the longitudinal and transverse development of UHECR-induced extensive air showers (EASs) investigators are gaining information on the primary composition, which favors light elements and disfavors a significant electromagnetic (e.g. photon) component. Such studies can also elucidate the high energy physics of the early interactions, which occur at center-of-mass energies well above that currently probed by accelerators[2].

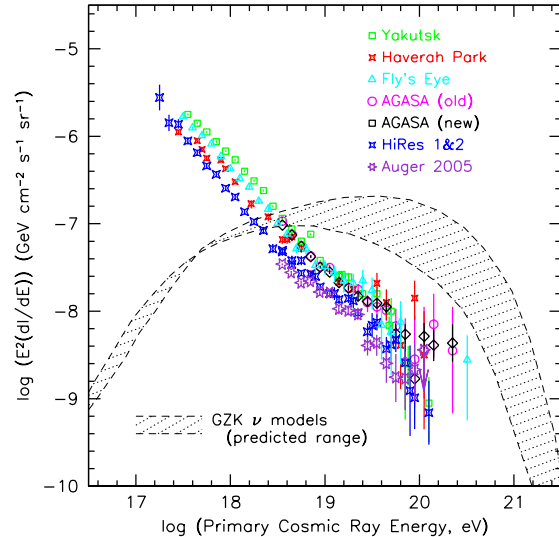The region near the endpoint of the UHECR energy

FIG. 1: *World ultra-high energy cosmic ray and predicted cosmogenic neutrino spectrum as of early 2006, including data from the Yakutsk [13], Haverah Park [14] the Fly's Eye [16], AGASA [7], HiRes [23], and Auger [26], collaborations. Data points represent differential flux $dI(E)/dE$, multiplied by E^2. Error bars are statistical only. GZK neutrino models are from Protheroe & Johnson [18] and Kalashev et al. [19].*

spectrum is shown in summary form in Fig. 1, where no effort has been made to correct the systematic offsets in the flux levels of the different experiments involved. Above 10^{20} eV, the event rate is of order 1 per km^2 per century, producing still only a handful of events per year close to this threshold in all existing UHECR observatories. As is apparent from the current world spectrum, constraints on the high energy tail or statistically compelling details of any putative cutoff above the current highest energies will still require years of observation. The need for much-improved statistics to address the primary issues currently under investigation all argue for expansions of and improvements on existing methods. Such issues include the detailed shape of the UHECR energy spectrum [6, 7] (including the presence, or lack thereof, of the GZK cutoff [8, 9]), energy-resolved primary particle composition [10, 11], and source production mechanisms (i.e. origins) [12, 20, 21, 22].

In addition, the virtual certainty of the extragalactic origin of these particles ensures an associated cosmogenic neutrino flux, generated via photohadronic pro-

cesses throughout the universe [17]. Hadronic cosmic rays above $\sim 10^{19}$ eV propagating in the 2.7K cosmic microwave background radiation (CMBR) exceed the threshold for resonant Δ^+ particle production through the GZK process, and the rapid decay of these unstable secondaries leads to pions and subsequently neutrinos. The mean free path of a 10^{20} eV proton in the CMBR is several Mpc in the current epoch, whereas the neutrinos are unattenuated from any cosmic distance. Future observations of cosmogenic GZK neutrinos will provide a unique and complementary view of the UHECR production, propagation, and attenuation throughout the universe, motivated by the UHECR observations themselves. Figure 1 shows also a band indicating the range of models for these cosmogenic neutrinos. The uncertainties in the models stem primarily from the details of the highest energy part of the UHECR spectrum, as well as the epoch of maximum UHECR source evolution, and GZK neutrino observations will thus provide independent constraints on the UHECR sources.

1.   Motivation for Microwave EAS Detection.

While there is general agreement among the different experiments as to the global properties of the UHECR spectrum, as Figure 1 shows, there is still significant disagreement and uncertainty on absolute flux scales and on some of the fundamental questions of UHECR research. The two primary techniques of UHECR observation, ground-based particle arrays and optical fluorescence detectors both suffer from tangible limitations. In the case of ground arrays, only a single slice of EAS longitudinal development can be observed. This means that determinations of primary particle energy and composition require extrapolation via model-dependent estimates, which may disagree depending on the model used. While the optical fluorescence method enables one to observe longitudinal as well as transverse shower development, it is highly constrained by the fact that it can only work on clear, moonless nights. This leads to a net yearly duty cycle of only 5-10%[24]. Furthermore, because the highest energy events are observed at increasingly large distances, even small fluctuations in atmospheric aerosol contamination can have substantial effects on energy estimation.

An air shower dissipates virtually its entire energy budget through ionization, producing a tenuous plasma with an electron temperature of order 10^5 K or more. The ionization and subsequent de-excitation of molecular nitrogen in the N_2^{+*} 1N and 2P states leads directly to the optical N_2 fluorescence now observed. The hot air shower plasma cools rapidly on 1-10 nanosecond time scales, distributing its thermal energy through collisions with the neutral molecules, primarily N_2, which has the largest cross section and number density. This rapid cooling process leads to additional excitation of rotational, vibrational, electronic valence, and other modes of kinetic energy distribution among molecules, many of which can also lead to rapid de-excitation and subsequent emission.

In turn, the hot electrons themselves, while producing this excitation, can produce their own emission, such as continuum bremsstrahlung emission, or recombination radiation. The fraction of total radiated energy in optical fluorescence, compared to the total available energy budget for secondary radiation, is very small, leaving much possible radiative energy still unaccounted for. The possibilities for observing secondary air shower plasma emission other than optical fluorescence have not yet been explored in any detail.

We propose here to expand investigations of the feasibility of other channels for EAS observations. To this end we have undertaken several experimental efforts, including two accelerator experiments. The promising results from these measurements have led us to commission a testbed prototype detector, which has helped to establish the methodology that could be used to make detailed measurements of EAS microwave molecular bremsstrahlung radiation (MBR)[28]. In this proposal we describe the accelerator results and the testbed development that has resulted from them, which we have dubbed the Air-shower Microwave Bremsstrahlung Experimental Radiometer (AMBER).

B.   Molecular Bremsstrahlung Radiation.

MBR in weakly ionized air is created by free electrons accelerating through collisions with the fields of molecules in the ambient medium. EAS ionization is considered "weak" since the interactions of free electrons or ions are dominated by collisions with neutrals rather than other ions. MBR has been classically treated as a thermal process, with the emission coming from ≤ 10 eV electrons assumed to be distributed with isotropic Maxwellian velocities. By these assumptions steady-state MBR emission is expected to be isotropic and unpolarized, which strongly differentiates it with the highly directional bremsstrahlung from relativistic particles which may be more familiar to a high energy or cosmic-ray physicist. MBR emission shares this property with optical fluorescence emission, an important feature which allows for the possibility of performing shower calorimetry by mapping the MBR intensity (and thus the ionization content) along a shower, much as optical fluorescence detections maps the nitrogen excitation along the same shower. As indicated in Fig. 2, MBR emission and optical fluorescence both are emitted in all directions around an EAS, and detectors may therefore "image" the air shower glow as a track along the sky to establish two-dimensional angular geometry, and use the timing information for the pulse arrival to determine the range evolution of the shower, giving a complete reconstruction of both geometry and particle number evolution.

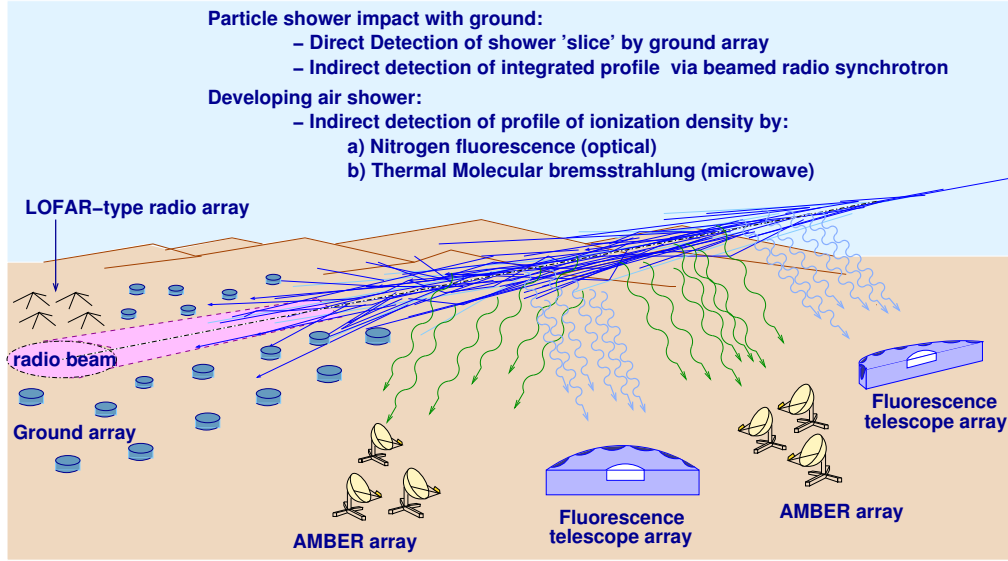The expected isotropic behavior of MBR is also in

FIG. 2: *Conceptual sketch of how microwave bremsstrahlung detection relates to other methods of ultra-high energy cosmic ray air shower detection.*

sharp contrast to *relativistic* radio emission processes such as Cherenkov, transition, or synchrotron radiation, all of which are beamed and highly polarized. In this respect it is convenient to think of MBR emission as analogous to "radio fluorescence," whereas beamed relativistic radio emission is closely aligned to the particle content of a shower and thus should be identified as concordant with the information derived from a ground EAS detector array. Furthermore, MBR intensity is expected to be proportional to the EAS ionization rate, which is known to be itself proportional to N, the total number of charged particles in the shower. This therefore leads to a direct relationship between MBR intensity and shower energy, with the degree of proportionality determined by the details of local correlations between electron velocities or radiative transitions in the tenuous air shower plasma.

The proportionality will depend on important details which require empirical determination, much the same way that oscillator line strengths necessary to understanding optical fluorescence must be determined via laboratory calibration with additional corrections for atmospheric conditions. For example, since an EAS produces an initial distribution of ionization which is likely to be a power-law rather than a Maxwellian, there are corrections for non-thermal effects such as stimulated emission and other non-equilibrium continuum radio emission channels, which may significantly increase the emission power over the minimal thermal MBR baseline. In addition, the cross sections for both elastic and inelastic collisions of electrons with air molecules are complex functions of electron energy, yielding strong velocity dependence in the electron collision frequency which can also contribute to MBR emission coefficients. Such effects are difficult to

analytically estimate and will be best calibrated *in situ* as has been done for other EAS observation methods.

To analytically determine the expected *minimum* flux density for MBR, we start with the emissivity from classical bremsstrahlung analysis of collisions between electrons and neutral molecules [28]:

$$\eta_\omega(u) = \frac{e^2}{16\pi^3\varepsilon_0 c^3}u^2\nu_{en}(u)\zeta(\nu_{en},\omega) \ . \tag{1}$$

Where ω is the microwave radian frequency, u is the electron velocity, $\nu_{en}(u)$ is the velocity-dependent electron-neutral collision frequency, and $\zeta(\nu_{en},\omega)$ is a term that accounts for the collisional suppression of radiation which arises from the destructive interference of fields from successive collisions within the radiation formation zone of each collision, a process also known as *plasma dispersion* [28].

Under the assumption of an isotropic and time-stationary velocity distribution,

$$\zeta(\nu_{en},\omega) = \frac{1}{1+(\nu_{en}(u)/\omega)^2} \ . \tag{2}$$

For an altitude of 5 km, $\nu_{en} \simeq 3$ THz at electron energies of about 2 eV, near the peak of the collision cross section; for room temperature electrons, $\nu_{en} \simeq 40$ GHz. The corresponding suppression factors are $\zeta \simeq 5 \times 10^{-5}$, and $\zeta \simeq 0.4$, respectively, showing the wide extremes of values possible under the range of electron temperatures that obtain in an air shower.

To preface further discussion below, we note that there are several other effects that compete with plasma dispersion and will tend to enhance the emissivity, or "suppress the suppression." First, stimulated emission, even at a
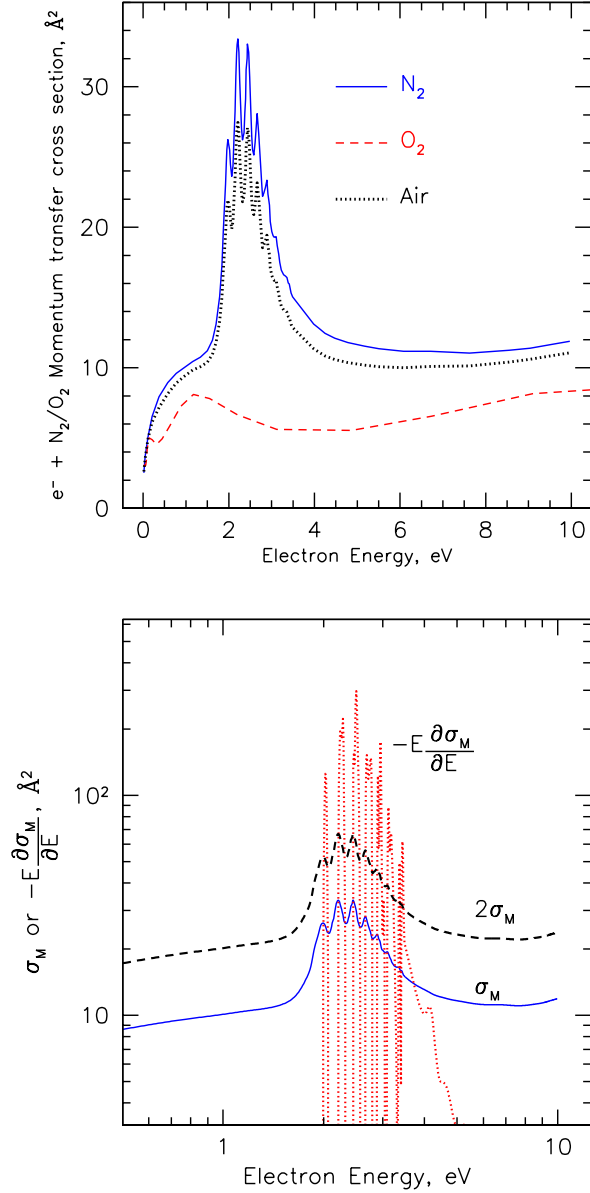
3

FIG. 3: *Top: Cross section for momentum transfer between electrons and N_2, O_2, and air over the energy range of interest for molecular bremsstrahlung production [36, 37]. Bottom: The red-dotted lines show the function $-E\frac{\partial\sigma_M}{\partial E}$ which must be greater than either σ_M (weak criterion; blue line) or $2\sigma_M$ (strong criterion, black-dash line) as a necessary condition for stimulated bremsstrahlung emission in an air plasma. See text for details.*

very small level, leads to correlations in electron-photon transitions. Such emission does not require a full-blown population inversion, as in laser processes, but rather deviations from the quasi-ground-state Maxwellian distribution can enable low levels of stimulated emission. Second, velocity correlations of the electrons due to the imposed geometry of the shower tracks and the anisotropic

distribution of ions can impose some cylindrical symmetry in the distributions, in tension with the assumption of uncorrelated isotropy in the electron behavior. Finally, weak plasma correlations on the scale of the Debye length can lead to coherent motion of electrons over very small scales, but large enough to overcome some fraction of the suppression effects.

To introduce an *ad hoc* accounting for the sum of all such effects, we impose a "coherence factor" ξ which modifies the ζ term:

$$\zeta_c(\nu_{en},\omega) = \frac{\xi}{1+(\nu_{en}(u)/\omega)^2} \quad . \tag{3}$$

where $\xi > 1$ parameterizes the level of excess emission above the "suppression floor" determined by ζ in the absence of any correlation of either electrons or electron-photon transitions. The term ξ can then be determined empirically to set the scaling of the emission, with $\xi = 1$ representing the MBR floor level.

The emissivity η_ω above must be integrated over the distribution of electron velocities to yield the emission coefficient j_ω (W m^{-3} (radian/s)$^{-1}$ steradian^{-1}):

$$j_\omega = \int_0^\infty \eta_\omega(u)f(u)u^2 \, du, \tag{4}$$

where $f(u)$ is the electron distribution function, which is Maxwellian in the thermal limit:

$$f(u) = \left(\frac{m_e}{2\pi kT_e}\right)^{\frac{3}{2}} \exp\left(\frac{-m_e u^2}{2kT_e}\right) \quad . \tag{5}$$

for electron temperature T_e. Similar analysis yields the absorption coefficient α_ω:

$$\alpha_\omega = -\frac{4\pi}{3c}\frac{\omega_p^2}{\omega^2}\int_0^\infty \nu_{en}(u)\zeta(\nu,\omega)\frac{\partial f(u)}{\partial u}u^3 du \tag{6}$$

where the plasma frequency is given by $\omega_p^2 = N_e e^2/(m_e \varepsilon_0)$ for electron number density N_e. These coefficients are combined to form the source function $S_\omega = (1/n^2)j_\omega/\alpha_\omega$ which is then integrated along a ray s through plasma column to the observer to determine the net intensity per unit radian frequency, or flux density I_ω:

$$I_\omega = \int_0^{\tau_0} S_\omega(\tau) \, e^{-\tau}d\tau \tag{7}$$

where the optical depth τ is defined by $d\tau = -\alpha_\omega ds$. Note that the absorption coefficient is not necessarily positive definite: under conditions where $\frac{\partial f(u)}{\partial u} > 0$, e.g., if there is an inflection in the electron velocity distribution function, then α_ω can become negative and stimulated emission will cause the radiation to grow with propagation distance.

The MBR flux density received by a ground detector is estimated by integrating the intensity thus derived over the

solid angle of the receiving antenna beam to yield Watts per m^2 per Hz over a given frequency band. The minimum detectable change in flux density for a radio antenna and receiver is [31]

$$\Delta I_{\omega,min} = \frac{k_B T_{sys}}{A_{eff}\sqrt{\Delta t \Delta \nu}}, \qquad (8)$$

where T_{sys} is the noise temperature of the receiver system, A_{eff} is the effective area of the antenna, Δt is the receiver sampling time constant, and $\Delta \nu$ is the receiver bandwidth. After passage of the relativistic shower front, the emission continues during the electron thermalization time, t_{th}. This time is determined by both elastic and inelastic collisions of electrons with air molecules [34, 35], giving $t_{th} \simeq 10$ ns for dry air at 1 atmosphere. The received radiation continues during the time the shower remains in the field-of-view of the antenna. At 4 GHz, for a D=1.8 m dish (giving $2\lambda/D \simeq 5°$), this time can be many microseconds for a distant shower.

Note that there is also a direct analog possible between an optical fluorescence detector which used photomultiplier "pixels" to image the two-dimensional projection of the optical fluorescence intensity along the shower, and a radio dish which can use an array of focal plane receiver feeds (each of which is effectively a pixel) to image the MBR intensity along the same shower. Feed pixel-arrays are not so common in radio astronomy because of the success of radio interferometry, but they are established technology where low-resolution bolometric imaging is important (for example, in submillimeter radio astronomy).

1. Departures from Equilibrium conditions.
Our estimates of the MBR emission of UHECR air showers using the standard thermal electron formalism here indicate that the energy threshold for detectability of the emission depends on the behavior of the modified suppression term ζ_c, which is affected by several classes of non-equilibrium conditions that can obtain in an air shower plasma.

a. Stimulated Bremsstrahlung. As an example of the departure from the assumptions regarding the velocity dependence of the electron collision frequency, Figure 3(top) shows the experimental electron-molecular nitrogen momentum transfer cross section σ_M in the energy range of interest. Most notable is the 2.3 eV resonance due to elastic collisions that lead to rotational excitation [36]. This resonance region is in fact the complement of what is observed in optical fluorescence–the energy transferred in this region of the cross section is released in part through optical fluorescence, and the complexity of it is in part mirrored in the structure of the optical nitrogen fluorescence transitions. Such highly nonlinear changes in collisional parameters with electron energy strongly depart from the assumptions used above, and similar effects have been found to lead to stimulated

emission even in highly collisional plasmas under some conditions [28].

In fact, stimulated bremsstrahlung emission from gas discharge plasmas was observed in the early 1970's and 1980's in a series of experiments [28, 29]. Necessary, though not sufficient, criteria can be stated for stimulated bremsstrahlung emission: $-E\frac{\partial \sigma_M}{\partial E} > \sigma_M$ for anisotropic electron distributions whose direction is parallel to the direction of the electric vector of the propagating radiation, and $-E\frac{\partial \sigma_M}{\partial E} > 2\sigma_M$ for isotropic electron distributions. Figure 3(bottom) evaluates this condition for the molecular nitrogen case shown in Fig. 3(top), and it is evident that both of the conditions above are strongly satisfied in the neighborhood of the resonance. Under such non-equilibrium conditions, an electron population inversion in the ionized region is possible, and this can lead potentially to stimulated emission [28]. Such inverted populations have been observed in discharge experiments in molecular nitrogen plasmas [32, 33].

b. Oxygen attachment. Molecular oxygen has a momentum transfer cross section significantly lower than that of nitrogen over this energy range, as shown in Fig. 3(top), and, after weighting for abundance, its effect on the overall momentum transfer cross section in air is minimal. Although O_2 does not contribute much to the thermalization of electrons in air, it does however play an extremely important role in removing free electrons once they have thermalized, since the three-body attachment cross section to O_2 rises steeply at low electron energies. In fact the attachment time scale for room temperature electrons is comparable to the ~ 10 ns thermalization time scale for hot electrons in 1-atmosphere air [38]. Once attached to ions, the electrons can no longer contribute to the bremsstrahlung continuum radiation. And since the initial spatial distribution of the oxygen ions is highly structured, and the ions are almost stationary in the short period during electron attachment, they impose a rapidly developing anisotropy in the *removal* of electrons from the free distribution, creating MBR in the free-bound transition. This effect also imposes anisotropy in the velocity distribution of the electrons.

c. Plasma correlations. The Debye length, over which an electron is fully shielded from a neighboring ion in a plasma, is given by $\lambda_D = \sqrt{\epsilon_0 k T_e/(e^2 n_e)}$. For an EAS plasma at an energy of 10 EeV or more, λ_D $1-2$ cm. Since over this distance there may be several hundred ion pairs along each relativistic through-going particle track, along with several hundred to several thousand tracks per square cm in the vicinity of the EAS core, electrons do not behave entirely independently but are subject to weak bulk plasma effects at some level which will produce phase-space correlations. For our case we may class these effects together with the attachment effects above; in either case the end result will be parameterized via equa-

tion 3.

2. Radiative Coherence.

While the field strength for a single electron is accurately described by the MBR theory, the summation of these fields in the presence of correlated velocities can significantly alter the resulting ensemble field strength. Such alterations, which may be produced by intrinsic shower geometry, or electron-photon correlations from stimulated emission, or by other plasma effects, still may be described via simple vector sums of the field strength of each of the radiating particles involved.

For individual emitters the resultant field strength will grow as a phasor sum [39]:

$$\vec{E} \;=\; \sum_{j=1}^{N} \vec{\varepsilon}_1(\mathbf{v}) \exp\left(-i\,\vec{k}\cdot\vec{x}_j\right) \tag{9}$$

where N_e is the total number of electrons in the plasma, $\vec{\varepsilon}_1(\mathbf{v})$ is the field radiated from a single electron, $\vec{k}$ is the wave vector of the radiation, and $\vec{x}_i$ is the position of the jth electron with respect to the observation point. The total radiated far-field power per unit area P/A is given by the magnitude of the Poynting flux $P/A = |S_{tot}| \;=\; |\vec{E}|^2/Z_0$ where $Z_0 \simeq 377\ \Omega$ is the impedance of free space. In the limit of complete coherence, the phase factors $\vec{k}\cdot\vec{x}_i$ are all unity, $|\vec{E}| \;=\; N_e\,\varepsilon_1$, and the total coherent power is $P_{coh} \;=\; N_e^2\,P_1$, where P_1 is the power radiated from a single electron. Since N_e is proportional to shower energy, the coherent power depends quadratically on the energy of the primary particle. In the incoherent limit, the sum of the phase factors corresponds to a two-dimensional random walk in the real and imaginary components of the resultant field strength, and the total power grows as $P_{incoh} \;=\; N_e\,P_1$.

While in general the partially coherent case requires a detailed knowledge of the electron phase space distribution function, we can get a qualitative sense of the behavior by considering a case where the N_e electrons consist of M subgroups of μ_e electrons each, such that $N_e = M\mu_e$. Assume that the μ_e electrons in each subgroup radiate coherently, but that the subgroups themselves are uncorrelated. Thus, while the radiated fields from the M subgroups add incoherently, the subgroup electrons themselves radiate coherently, and the resulting *partially* coherent power is $P_{part} \;=\; M\,\mu_e^2\,P_1$, now quadratic in μ_e rather than N_e. The ratio of the partially coherent power to the incoherent power is proportionally

$$\frac{P_{part}}{P_{incoh}} \;=\; \frac{M\,\mu_e^2\,p_i}{N\,p_i} \;=\; \mu_e. \tag{10}$$

Similarly the ratio of coherent-to-incoherent power grows as N_e. Since the plasma density of ionization electrons in a shower scales linearly with shower energy, both the coherent and partially coherent regimes will yield radiated

power that grows *quadratically* with shower energy. In fact, as soon as $\mu_e \geq 10$, coherence begins to dominate over the incoherent component by an order of magnitude or more. Even modest correlations among the shower ionization electrons can thus rapidly lead to much larger detected emission than expected.

We have parameterized these effects using the correction term ξ which modifies the collisional decoherence factor ζ as described above. In practice empirical data will be required to establish the emission constants associated with these factors, as is the case for all other emission mechanisms in a real air shower.

C. Accelerator beam tests.

Motivated by the fact that even the floor level of fully-suppressed emission from the MBR process appeared to us to be detectable under air shower plasma conditions, we have performed two accelerator tests designed to measure the MBR in a laboratory air-shower plasma. In these experiments we have found good evidence for microwave continuum emission with characteristics suggestive of a major departure from the standard incoherent MBR emission scenario, not an unexpected result given the variety of different non-equilibrium, non-thermal, and partially coherent processes that are possible. We detail these results here.
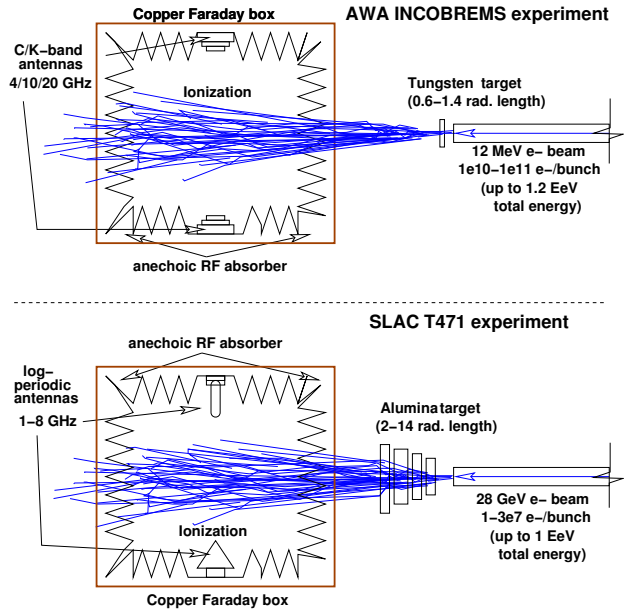

FIG. 4: *Schematic of AWA INCOBREMS (top) and SLAC T471 (bottom) experiments, which used electron beams to shower in either Tungsten or alumina targets to produce ionization inside an anechoic Faraday chamber, observed by internal antennas.*

1. AWA INCOBREMS.

In June 2003, the INCOBREMS experiment was performed at the Argonne Wakefield Accelerator (AWA). For this experiment, energetic γ-rays were produced by bombarding several thicknesses of tungsten target with a 12 MeV electron beam with pulse
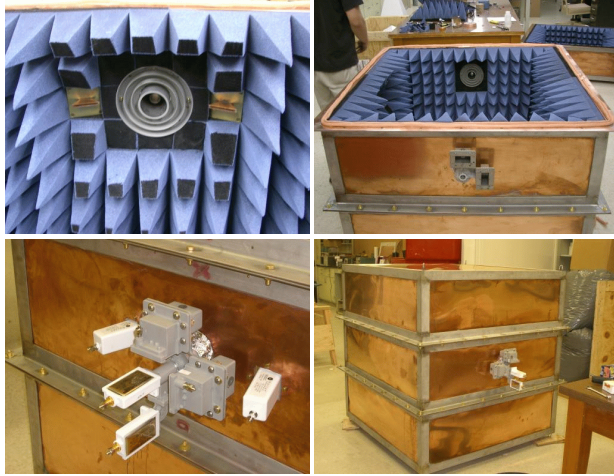
FIG. 5: *Views of the exterior and interior of the Faraday anechoic chamber used for measurements of microwave continuum emission in the INCOBREMS and T471 experiments. The box is approximately a 1 m cube in dimensions.*

charges of 0.1-1 nC. The γ-rays were then used to ionize air in a 1 m^2 copper anechoic Faraday chamber equipped with C, Ku, and Ka-band antennae, producing the equivalent ionization of a PeV electromagnetic shower inside the Faraday chamber. Figure 4 shows a schematic view of the general layout in the two experiments, and Fig. 5 shows several views of the anechoic Faraday box employed in both cases (here shown with the antennas and receivers used for the first experiment).

In Fig. 6 (top), we show results of the AWA measurements at 10GHz (Ku-band). Both incoherent and phase-stable (at least partially coherent) emission components were observed for tens of nanoseconds after beam passage. The total energy of the incoherent component was consistent with thermal MBR. Problems with beam scraping backgrounds necessitated difficult background subtractions, leading to doubts about the reliability of the results, so another experiment with a cleaner beam was scheduled at SLAC.

2.   SLAC T471/E165.   In the following year, a similar experiment, T471, was performed at the Stanford Linear Accelerator Center. The configuration of this experiment was largely the same as that of INCOBREMS, but additional precautions were taken against EMI and beam backgrounds, and verified in lab and beam calibration tests. This experiment was coordinated to be operated just downstream of the E165 FLASH experiment, which was used to do precise calibration of air fluorescence for the HiRes collaboration [30]. The SLAC T471/E165 experiments also used a precisely controlled, 28 GeV electron beam which was collided with a target consisting of 90% Al$_2$O$_3$ and 10% SiO$_3$ to make showers with varying particle number, from 0 to 14 radiation lengths of material.

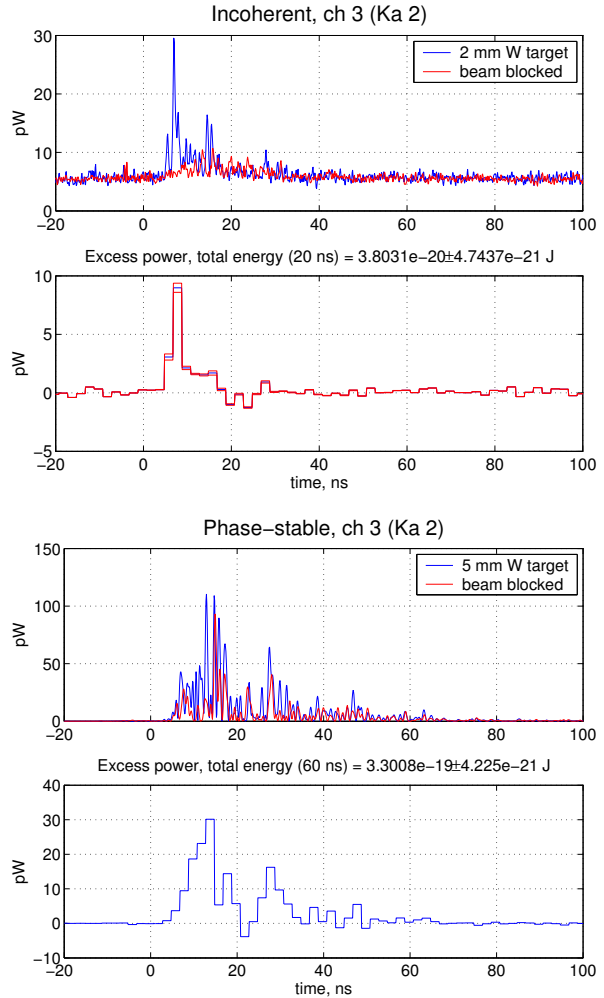Figure 7 shows preliminary results from measurements

FIG. 6: *Top pair: Best estimates of observed phase-incoherent component of emission for a 2mm tungsten target during the IN-COBREMS experiment at AWA, at 10 GHz. Bottom pair: Phase-stable (partially coherent) component for a 5mm tungsten target, an order of magnitude larger than for the incoherent case. Upper panes in both pairs show blue as total emission and red as the background due to stray ionization from the beam; lower panes show the background-subtracted results.*

of the emission over the 1.5-6 GHz band, using an antenna that was co-polarized with the electron shower momentum. Here the square of the average signal voltage is plotted vs. the time after beam entry into the Faraday chamber. The transit time for the chamber is about 3.3 ns for the beam. An initial strong impulse is observed at the first causal point in time after beam entry. This impulse is found to be highly polarized with the plane of polarization aligned with the beam axis and Poynting vector, characteristic of transition and radio Cherenkov radiation. Such emission was anticipated, and is damped almost immediately due to the microwave absorber ($\geq$ 30 dB per reflection even at angles of order 55° from normal incidence) that covers the interior of the Faraday chamber (the im-

SLAC T471, July 2004

1.5−6 GHz, co−polarized
T_{sys} = 400K
100 beam shot avg.

scope noise level

SLAC T471, July 2004

1.5−6 GHz, cross−pol.
T_{sys} = 400K
100 beam shot avg.

ΔI, 1 shot

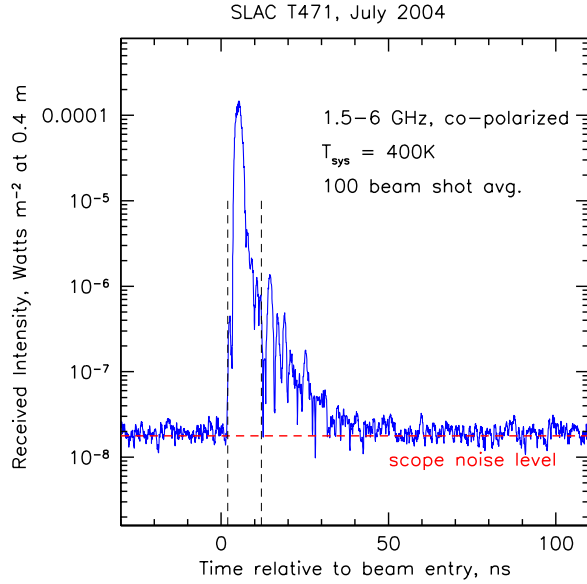ΔI, 100 shots

MBR,
no suppression

MBR,
full suppression

FIG. 7: *Average microwave emission amplitude from 100 beam shots taken near shower-maximum in the 2004 SLAC T471 experiment, using a broadband antenna that was polarized along the electron beam axis, and was thus sensitive to partially coherent radiation directly from the relativistic electron shower as it transited the Faraday chamber. A strong initial pulse is seen, with rapid decay, followed by a second exponential tail with a longer decay. The noise level is in this case determined by the limited dynamic range of the oscilloscope used, rather than the thermal noise level.*
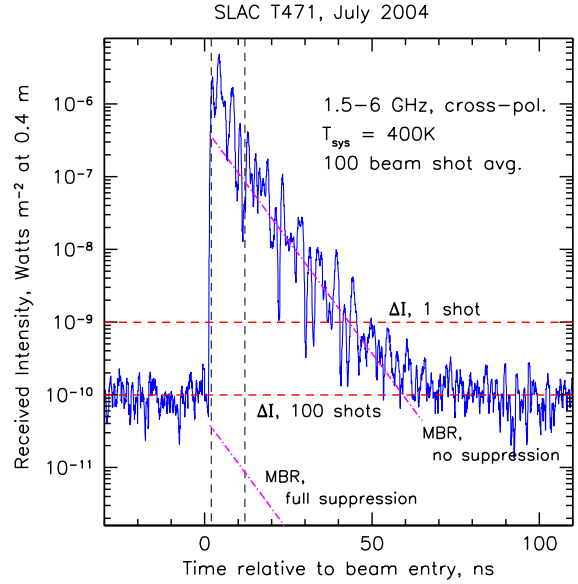
FIG. 8: *A plot similar to the previous figure, but now using a cross-polarized antenna which was insensitive to radiation polarized with the electron beam. The dynamic range of the system was now improved so that the noise level is determined by thermal noise, and the detected microwave emission extends out to 60 ns or more, with an exponential decay time constant of about 7 ns. The upper and lower dashed red horizontal lines indicate the minimum detectable intensity, as given by equation 8, for the single-shot case, and the 100-shot average. The diagonal dot-dash lines are the two extreme-case estimates for MBR emission: the upper case for no net collisional suppression and the lower case for maximal collisional suppression of the emission, both for the case where the electron thermalization time constant is the source of the 7 ns exponential decay observed.*

plied average time constant for quasi-exponential decay of reflections is of order 1.3 ns for this absorber in this geometry). The noise level in this plot is dominate by digitization noise, since the sensitivity had to be reduced in order to achieve enough dynamic range to see the strong initial impulse.

In Fig. 8 we plot the same measurements made with a cross-polarized antenna, which was therefore insensitive to the relativistic shower emission. In this case the strong initial impulse is not prevalent, and the exponentially decaying emission extends out to 60 ns or more, with noise levels now determined by the thermal noise level rather than scope noise. Based on measurements, no beam-related background was present, and thus no background subtraction was necessary. Several curves are also plotted with the data. The horizontal lines indicate the thermal noise level for single shots and for the average of the 100 beam shots used here, based on equation 8 above. The diagonal dot-dash curves are model predictions based on equation 7 above, calculated for the two extreme cases of the collisional term ζ_c from equation 3, one for the case of no suppression ($\zeta_c = 1$) and the other for full collisional suppression ($\xi = 1$). It is evident that, if MBR is responsible for this emission, the collisional suppression is almost

completely offset by the partial coherence.

The radiation observed in T471 is also partially coherent. This is shown in Fig. 9, which plots the observed microwave energy vs. integrated microwave power from 15-30 ns after the pulse. The quadratic correlation here indicates that the partially coherent portion of the emission dominates completely over incoherent emission. The coherent emission appears to be several thousand times the expected incoherent emission level, implying that subgroups of $\mu_e \simeq 30 - 50$ electrons are radiating coherently within their subgroup, using the notation of section I B 2 above. Given that the showers used in T471 created of order 10^{12} electrons within the Faraday chamber used, the net correlation is still extremely small compared to the total, and it is evident that this level of partial coherence is very far removed from the full-spatial coherence that obtains in coherent Cherenkov or transition radiation.

3.   Scaling to air showers.   Under the assumption that standard radiation scaling laws obtain, we can make an estimate of the threshold for detectability of the emission seen in Fig. 8, if we scale it to air shower observation
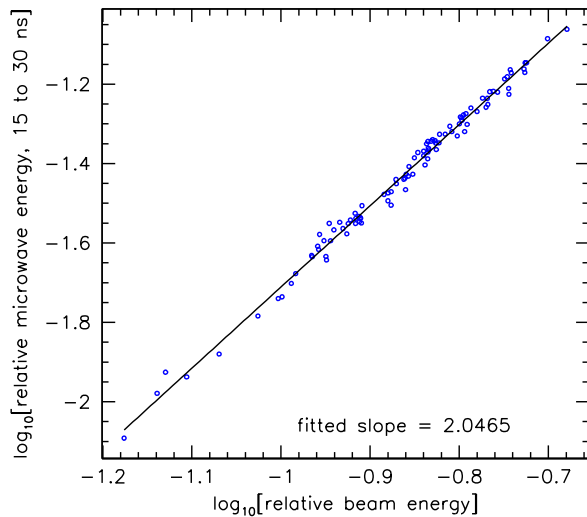
FIG. 9: *Plot of relative microwave energy in the tail of the observed air plasma emission vs. the relative microwave energy observed in an external transition-radiation monitor of the beam current, which is directly proportional to beam energy. The observed microwave power follows closely a quadratic rise with beam energy, characteristic of coherent radiation.*

distances and a realistic detection system.

To do this, we take the flux density as estimated from the data in Fig. 8, using the weighted average T471 antenna effective area of 0.05 m^2. Using this flux density and the equivalent shower energy of 3.4×10^{17} eV, we scale to an equivalent air shower at a distance of 10 km. The scaling corrects for the lower electron density expected for a typical 5 km air shower altitude. We also assume an integration time (several hundred ns) based on angular transit times for showers at roughly this distance, with the peak flux density determined by the emission over an interval comparable to the thermalization time. We consider both linear and quadratic scaling of the emission with electron density, and with regard to the shower geometry, as long as the transverse diameter of plasma column is contained within the antenna beam, we assume there is a direct scaling from the T471 observations to air shower observations.

The results of this analysis indicate that, if the partially coherent emission observed in T471 scales only linearly with shower energy (as might be expected in the pure "incoherent" case), then the threshold of the AMBER system at 10 km is of order 8×10^{18} eV in shower energy. If the scaling is quadratic with shower energy, as the data suggests, the threshold is lower, of order 1.6×10^{18} eV.

We can also estimate the maximum distance to which a shower at the GZK threshold energy of 3×10^{19} eV could be observed under these same conditions: for the linear-scaling case, the distance is of order 20 km; for the quadratic case it is much larger, of order 200 km, but of course in this case earth-curvature and atmospheric attenuation would also require consideration. In either case, the current emission parameters strongly warrant further investigation of the potential for development of MBR detection of air showers.

4. Beyond detection: Shower Calorimetry with an AMBER array.

The importance of MBR detection of EAS rests in the potential that it will yield the observational advantages comparable to those of optical fluorescence without the shortcomings associated with weather and limited duty cycle. By observing MBR, one is observing an EAS from the same perspective as with optical fluorescence, via energy-loss processes that are intimately related to the excitation of molecular nitrogen that leads to air fluorescence. However, observations can occur 24 hours per day, and at the microwave bands of interest there is virtually no attenuation due to atmospheric contamination from aerosols or clouds. Even heavy rain leads to attenuation of ≤ 1 dB above elevation angles of $30°$ at C-band (4-6 GHz), a 20% effect. Initially, while the MBR technique is being cross-calibrated with respect to an optical fluorescence and ground array, this immunity to atmospheric effects can yield immediate benefits in helping to extrapolate the energy scale for distant events, where optical fluorescence is most affected by aerosols and other atmospheric uncertainties.

Commercially designed microwave reception equipment can be easily weatherproofed, and future arrays would most likely be able to employ off-the-shelf satellite television components, taking advantage of the tremendous economy of scale in wireless and satellite television technology. Following validation of the technique in coincidence with an existing EAS installation, MBR detectors could be potentially deployed as standalone UHECR observatories. Critical to the success of such an observatory is the ability of MBR to do precision shower calorimetry. There appears to be good initial evidence from the T471 experiment that such calorimetry can be done with precision that is comparable to current techniques.

Referring to Figure 9, we stress that individual single-shot measurements of the integrated microwave energy in the shower can be used to determine the beam energy in the experiment to about 2-3% precision, once the overall energy scale is set (in this case by an external beam current monitor). This level of precision is set entirely by the instantaneous signal-to-noise of the data, and is not systematics-limited, as evidenced by the precise quadratic scaling observed. In the T471 experiment, this scaling was observed over more than a decade (not shown in Fig. 9) of energy. In addition, the same scaling was seen at many different relative plasma densities (created by sampling the shower at different depths of development) in the

9

experiment, indicating that it is not dependent on shower age. Such results give us good confidence that, with sufficient attention to careful detector and system design, and adequate calibration, an MBR observatory could provide shower calorimetry which was comparable to that of existing techniques.

EAS observatories have also demonstrated capabilities for neutrino observations, but will require substantial increases in their apertures before such techniques can become practical in elucidating the GZK neutrino spectrum. Neutrino-induced showers are also likely to be highly-inclined relative to typical proton showers, and thus become problematic for observation with ground arrays, which suffer from more severe systematics at high zenith angles. In contrast fluorescence methods (and possibly the MBR methods we describe here) can readily observe such showers, since the geometry is no less favorable for horizontal than for vertical showers. Thus MBR observations may help to greatly expand the neutrino apertures of air shower observatories, by extending the duty cycle for "quasi-fluorescence" observations, perhaps by an order of magnitude or more.

D.   The AMBER system.

Following the indications of stronger-than-expected emission from the two accelerator experiments detailed above, we have moved ahead to develop a prototype of a system that could be used to search for detectable microwave emission from actual air showers. This system is built around a custom compact-PCI digitizer and data acquisition system, which we designate the Radio Bremsstrahlung Impulse Detector (RaBID). We have chosen the components and size of the prototype system such that it can be duplicated at low cost with mostly commercial parts. The proposed system, incorporating the RaBID prototype, is designated the AMBER for Air-shower Microwave Bremsstrahlung Experimental Radiometer. AMBER is currently operating on the rooftop of Watanabe Hall at the University of Hawaii at Mānoa (UHM) in Honolulu, Hawaii, pictured in Fig. 10. In its current configuration, the AMBER unit consists of a dual-band (C and Ku), dual-polarization feed horn array at the prime focus of a 1.8 m off-axis parabolic dish. The array is in a diamond-shaped configuration where each feed is $\sim 5.2°$ from its nearest neighbor. Each feed produces four channels of signal which are amplified and down-converted in Low Noise Blocks (LNB) and then conveyed to the RaBID DAQ via RG11 coaxial cable, as shown in Figure 10. The RaBID DAQ consists of a pair of RaBID cards located inside a compact PCI (cPCI) crate, along with a cPCI CPU for data collection and logging. At the RaBID card input, the down-converted LNB outputs are measured with RF power monitor (MAX4003) chips, which provide output proportional to the received RF power, with approximately 70 ns integration time. This power level is sam-
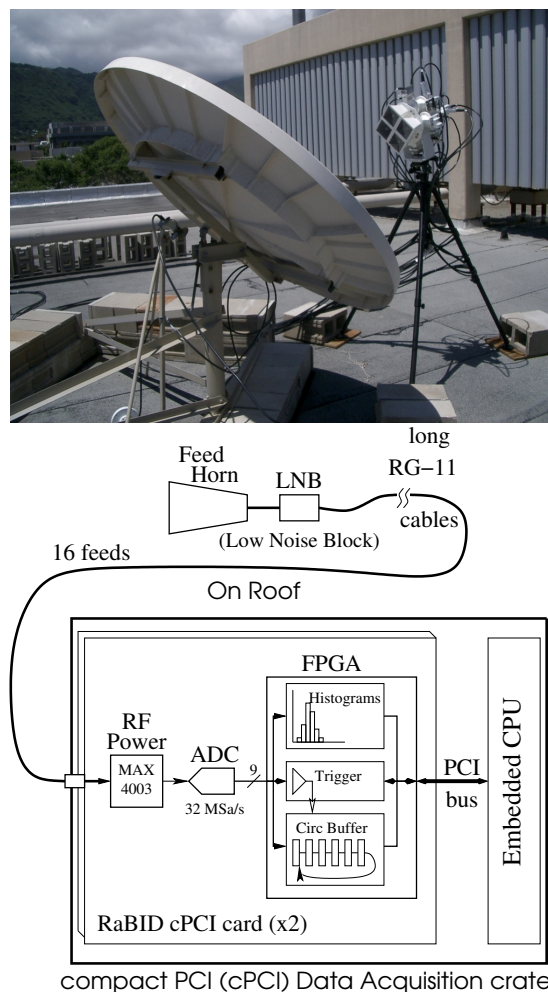

FIG. 10: *Top: Prototype AMBER telescope and feed array on the roof of the physics building at UHM. Bottom: AMBER detector readout chain. The feed horn signals are amplified and down-converted in a Low Noise Block and then transmitted to a pair of RaBID cards for processing. See text for details.*

pled with a 32MSa/s ADC and processed inside a Field Programmable Gate Array.

These digitized samples are processed in 3 parallel paths: (1) all C-band samples are logged into a hardware histogrammer, which allows optimum threshold-riding with varying background (2) a trigger threshold is set based upon the histogram values; and (3) a circular buffer holds the samples in time sequence to be read out into the CPU upon detection of a trigger condition. In order to avoid biases in the triggering, each feed horn channel (of 12 total) is triggered separately, at minimum possible threshold, and the trigger times (corresponding to different transit times across the array field of view) are analyzed in the stored data. All sample times are recorded with respect to a common clock, which is synchronized to GPS via Network Time Protocol. An external trigger port (not shown) is available for forcing readout when observ-

ing in conjunction with another detector.

1. AMBER Results.   Since initial commissioning of the AMBER system began in mid-2005, we have accumulated about 8 months of data under stable operating conditions, most of which has been analyzed to search for EAS-like events. Because AMBER lacks a ground-truth EAS array to validate any observed signals, any candidates that are observed remain only putative at best. However, we may test a sample of such candidates for similarity to expectations from our simulations, and we have done this for a large data sample taken through the spring of this year, with results that support the potential for EAS measurements by an AMBER array.

Data analysis for AMBER events involves several steps which significantly improve the signal-to-noise ratio of the raw data. First, because the MBR signal is by nature unpolarized, we can combine the recorded power in the two independent polarizations, improving the SNR by a factor of order $\sqrt{2}$. Also, the signal arrives over many sequential 70 ns time bins, whereas a significant fraction of the noise is broadband and largely uncorrelated between successive time bins. These statements are equivalent to saying that the spectral bandwidth of the signal is much less than that of the noise, and under such conditions we may apply Wiener filtering (also known as *optimal* filtering) to remove the out-of-band noise component, and properly weight the in-band noise components.

Examples of the effects of this analysis are shown for a candidate event in Fig. 11. On the left side the raw event that triggered the system at C-band (4 GHz) is shown, with the upper (earlier) signals from feed 4 and the later signals from feed 1 (lower left), indicating a downgoing event. On the right-side panes, the signals are shown for the combination of polarization co-adding and Wiener-filtering, with a marked improvement in overall SNR and resulting timing. Although the actual range to the event cannot be determined directly, we calculate a pseudorange based on the assumption that the feed-crossing signals were moving at the speed of light over the known angle between feeds. These pseudorange values can then be compared to simulations for actual EAS events.

Over the several months' observation period where the data has the highest quality, we have selected a sample of candidate events based on criteria derived from EAS expectations. Additional examples of such candidates are shown in Fig. 12. Here the projected elevations and azimuths for each feed are shown in each event pair. We find that downgoing events predominate in our current sample. This is expected from a true EAS sample, but without an independent air-shower tag for any given event, we cannot yet reject the possibility of anthropogenic origin.

We can however compare the derived pseudorange distributions for both simulations and actual data to determine if the candidates observed in our event sample are
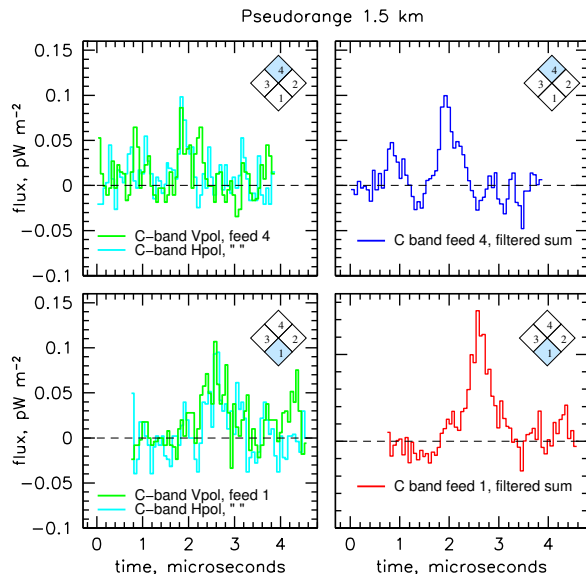

FIG. 11: *Example of an event recorded recently with the prototype RaBID system in Hawaii. The two events occurred sequentially in the two feeds noted, and triggered both polarizations at both feed 4 (top) and feed 1 (bottom), creating a downgoing event trigger. Left,: Raw data, showing peaks in both H and V polarizations for the C-band feeds. Right: Signal after co-adding the polarizations and applying Wiener filtering to remove the high frequency thermal noise fluctuations. The pseudorange is based on the 680 ns dual-feed crossing time.*

drawn from a distribution that is consistent with what is expected from actual EAS events. To do this we have developed a Monte Carlo simulation code from which we can extract the pseudorange value for events with various detectability thresholds and an energy spectrum consistent with the known UHECR energy spectrum.

Results from this analysis are shown in Fig. 13. The upper pane shows the simulations for two energy threshold at a distance of 10 km, and the lower pane shows the results for a sample of current candidate events. While these candidates cannot be proven to be EAS events without independent evidence from an air shower array, they do appear at least consistent to first order with the expectations from EAS events, and they demonstrate that an AMBER array has the basic detector characteristics to make measurements that are necessary to establish MBR observations as a viable EAS detection methodology.

In summary, we have proceeded as far as possible with MBR studies in the absence of coincident EAS ground-truth array measurements. We have provided compelling arguments that our current results merit further investigation in a dedicated experiment alongside an EAS observatory such as the Auger Observatory. We have considered carefully in this proposal the set of resources that we will require to do this. In the remainder of this proposal we present the details of our plan.
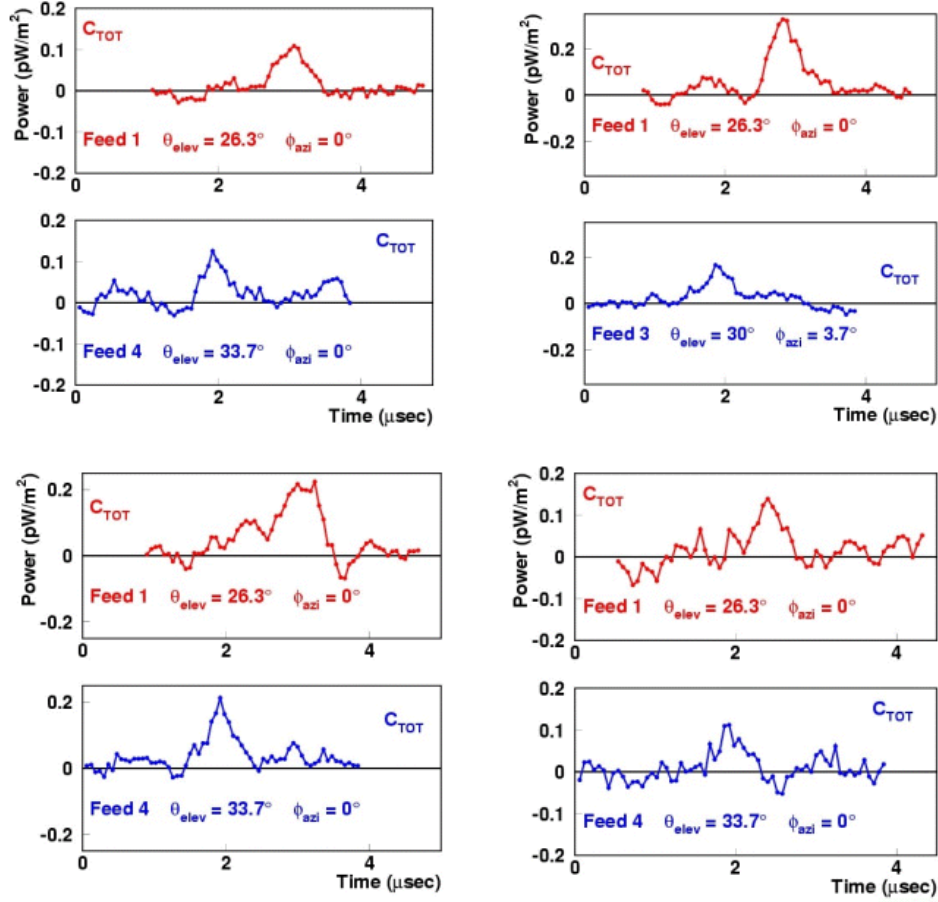
11

FIG. 12: *Examples of other events recorded by the prototype AMBER system, meeting the criteria for EAS candidates.*

E.   Plan of Deployment.

We propose to fabricate and deploy a four-antenna AMBER array, with slightly larger apertures, 2.4m compared to our 1.8m prototype, to improve the SNR and focal-plane scale. The antennas would be sited at the Southern Auger Observatory *Los Leones* Fluorescence telescope site. The antennas would be placed adjacent to the current facility and would be provided with a small dedicated space within the facility to house the supporting electronics.

The telescope boresights are chosen to match up with the directions of one of the North-easterly-pointing Auger fluorescence telescopes. In this configuration there is the best possible overlap with the ground array, as is indicated in Fig. 14. Here the edges of the fields-of-view of the Los Leones fluorescence telescopes are indicated with the red lines, and the telescope with which we would arrange geometric coincident is centered at $\sim 20°$ east of N. The feed arrays of the AMBER telescopes cover about 10° from edge-to-edge, but are arranged with approximately 8° offset in azimuth to align with the fluorescence boresight and to provide some overlap with adjacent AMBER telescopes. The pie-slices in Fig. 14 indicate the 15 km

range coverage of each of the AMBER feed arrays, covering an area of 50-60 km^2. For a 10 EeV threshold energy at 10 km distance, we expect a rate of 300-500 events per year, with about 5-10% coincidence with the fluorescence telescope, and a much larger fraction with the ground array. Such event rates will allow us to quickly ramp up our understanding of the potential of this method for future large-scale EAS observations.

P. Gorham currently has ongoing research and development funds via his 2002 Department of Energy Outstanding Junior Investigator (OJI) award which are available as seed funds for a variety of topics in Radio Detection of High Energy Particles, including this one. These funds have been used in support of the AMBER prototype, but the scope of this support is limited to seed funding for a larger scale effort.

A portion of these ongoing funds can and will be made available if necessary during the consideration phase of this proposal to ensure that crucial near-term tasks will continue to be addressed up to the decision point by the potential sponsor. This will help lead to a rapid transition to production and fabrication by continuing the effort in the following areas: [1] Development of a cost-effective
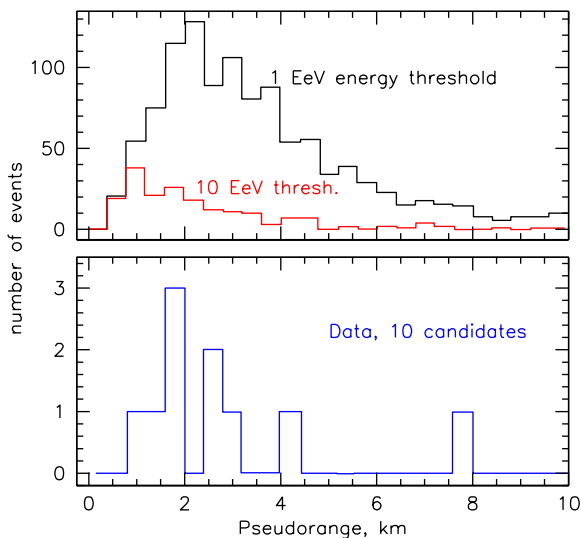
FIG. 13: *Upper: Pseudorange distributions of simulated events for an AMBER array with a 1 EeV energy threshold at 10 km distance (upper curve) and a 10 EeV threshold at 10 km (lower curve). Lower: Pseudorange distribution of 10 candidate events measured in recent AMBER data taken over several months.*
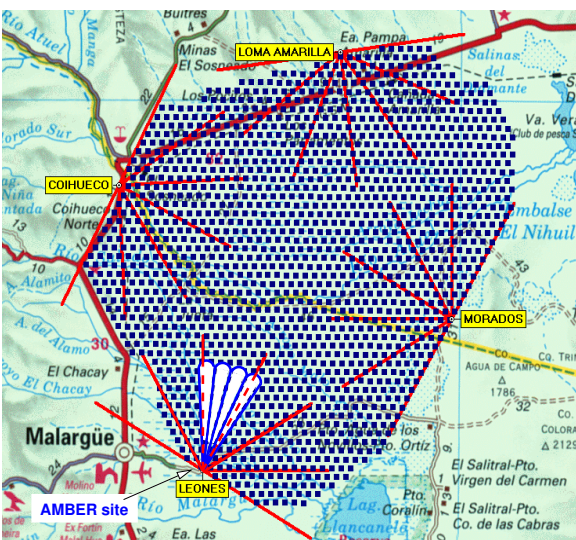

FIG. 14: *The larger scale arrangement of the locale of the Auger/AMBER site, with coverage of the AMBER telescopes indicated by the pie slices which are about 15 km in range from the deployment site, and cover a region of the array that is fully instrumented, and coincident with the field of view of a single Auger fluorescence telescope.*

mount structure for the arrays; [2] Firmware development to prepare for an external trigger from the Auger DAQ; [3] Development of field calibration equipment that can be used remotely; and [4] Further development of AMBER Monte Carlo simulation code.

The Ohio State group has obtained one-time funding of up to $50K to seed its work on AMBER. This sup-

port has been granted by the University's new Center for Cosmology and Astro-Particle Physics, recently selected for a significant infusion of university central funds in a campus-wide competition. These funds will be available to prepare the necessary infrastructure at the Auger site, to procure components for the AMBER telescopes, and to support other AMBER- related activities. These funds are also available if needed during the consideration period for this proposal.

Completion of the installation, followed by commissioning and initial debugging of the array can be expected to complete the third fiscal quarter of the program. Our hope is that three to four months of usable data could then be obtained by the end of the first fiscal year. Once the AMBER array is operational, data acquisition can begin with the aim of accruing at least one full year of initial data co-incident with air shower events. At this stage, depending on the indications in the data, the decision to continue for a third year would be made in conference with the sponsor and a review from the Auger project as well. This data will consist of three distinct subsets: [1] *Internally triggered sky data.* This data will be independently acquired by AMBER's on board triggering criteria. [2] *Externally triggered sky data.* This data will be dependent upon triggers issued by the Auger fluorescence and ground arrays. [3] *Calibration data.* Calibration will be done by pulsing the feeds with a stable RF source.

Detection of coincident events with sufficient confidence will give the first ever observation of broadband microwave emission from an air shower ionization region, and would lead in short order to estimates of the energy-scale and capability of the technique, because of the strong capability for cross-calibration that will be afforded by co-locating the array with the Auger observatory. Conversely, a lack of any coincident events will set the first limits on incoherent or partially coherent microwave emission from air showers, and provide a first lower limit on the shower energy required for such observations. In either case, the result will be disseminated through a comprehensive journal article to establish for all future investigators the utility of these potential techniques.

F.   Broader Impacts: Quarknet and AMBER.

We conclude the project description with a discussion of the broader impacts of the proposed activity. The major focus of this section is our partnership with the University of Hawaii QuarkNet center, first established in 2003. We choose to focus our efforts in developing these educational activities exclusively on Hawaii teachers and students, both to avoid spreading our resources too thin, and because Hawaii's students population includes a larger fraction of underserved minority individuals than in many US locales.

To address the challenge of using our AMBER efforts

to create a quantifyable impact on education in Hawaii, we propose to become a contributing partner to the existing QuarkNet Center which is now established in the University of Hawaii Department of Physics and Astronomy, led by Prof. Arnold Feldman, who specializes in Physics Education. We will contribute time from the Principal Investigator and UH AMBER co-Is G. Varner and P. Miočinović in support of the mentoring, and development of AMBER-specific elements of the current experimental infrastructure that is a strong element of the current QuarkNet program.

1. Hawaii's underserved K-12 students. Hawaii K-12 students have consistently shown poor performance compared to national averages in math and reading. [41]. Although Hawaii students are not routinely tested for science, clear evidence of below-average math/reading and science skills is provided by a 1996 report of the National Assessment of Education Progress (NAEP) which found that Hawaii students ranked 37th of the 40 participating states in science test results. [40]. A typical result of this study found that among eighth grade students found only 15% of them were proficient in science skills, compared to 27% in the national average, and 58% were "below basic" compared to 40% nationally.

One factor that has a direct impact on the students' performance is the fraction of time that Hawaii teachers themselves spend in science curricula, compared to the national average. In a recent study by Feldman, Campbell, & Lai [41] which surveyed more than a hundred Hawaii teachers of grades 4-6, the average time for science teaching was 77 minutes/week, which is more than 40% below the national average of 135 minutes per week. [42].

A partnership of AMBER and QuarkNet is in an excellent position to have a measurable impact on this deficit, through support of programs aimed at providing teachers with exciting new resources which will seed new curriculum development and provide hands-on experience with science and technology for high school students.

2. QuarkNet background. QuarkNet is an education and public outreach program sponsored by the National Science Foundation (NSF Grant ESI-9819486). and The Department of Energy Office of Science, and administered and coordinated through Fermi National Accelerator Laboratory. Its mission has best been summarized through statements provided by the project's own website (http://quarknet.fnal.gov):

> QuarkNet brings high school students and teachers to the frontier of 21st century research that seeks to research some of the mysteries about the structure of matter and the fundamental forces of nature... Physicists mentor and collaborate with high school teachers. Through these collabora-

tions students learn fundamental physics as they analyze live online data and participate in inquiry-oriented investigations. Teachers join research teams with physicists at a local university or laboratory.

Ultra-high energy cosmic ray and neutrino physics provide and excellent opportunity to inspire the vision of both teachers and students through development of an understanding of the nature of these particles which are both ephemeral and yet of critical importance in many astrophysics phenomena. Providing an understanding of how to envision and detect a form of matter than can penetrate through thousands of km of solid earth is an exciting challenge which will align well with the QuarkNet mission.

The AMBER PI has been supportive in the QuarkNet development at UH since its inception. Gorham was involved in some early development work for high-school-based cosmic ray detectors through the Caltech-managed CHICOS (California High School Cosmic-ray Observatory) (http://www.chicos.caltech.edu/) project, which now involves more than 55 different high schools in the Southern California basin. The concept of an internet-connected set of cosmic ray detectors located at different high schools and allowing teachers and students to form their own networked science community was the vision that helped to begin the UH QuarkNet center. The connection to cosmic ray physics and astrophysics also provides a strong initial scientific link to AMBER, and a framework on which to build an even stronger connection.

3. Proposed QuarkNet contributions. We propose to augment the current cosmic-ray detector fabrication projects with the development of a microwave detection system that will be a simplified version of AMBER, designed to give teachers and students the opportunity to transform conventional satellite TV equipment into interesting experiments in radio science. This is a topic of great relevance in a world increasingly dominated by wireless radio technology.

We propose funds for three such prototype systems, one per year, that would become centerpieces in the summer QuarkNet program at UH Manoa. QuarkNet teachers participate in a summer workshop for several weeks, during which they conduct hands on fabrication of hardware that is related to cosmic-ray research. Our component would add a module during the summer which would involve these teachers in the construction of a small CATV telescope similar to the AMBER system, which we designate AMBER-lite.

AMBER-lite will have a simplified four-feed array at the focus, enabling students to observe the behavior of microwave power in anthropogenic transients, and from solar transits across the array. Although the system will likely be too small for direct detection of cosmic ray events, it will provide a teaching tool for understand-

ing of radio and microwave energy, and will give a practical intellectual foothold for students trying to understand the AMBER application to high energy cosmic rays. AMBER-lite events will be archived on a desktop computer which will provides control, analysis, and networking software to link each school's system to the other schools. In addition, AMBER-lite's QuarkNet data will be made available to a wider component of QuarkNet's outreach system: a web-based data "Grid Portal" (http://quarknet.fnal.gov/grid) which will collect and make available data from QuarkNet centers across the country to teachers and students.

The current UH QuarkNet program had its first teacher workshop last summer, with 10 teachers participating in a mix of lecture and hands-on lab sessions. The lectures provide particle and cosmic-ray physics education for the teachers, earning UH graduate credits, which in turn allow for their own career (and payscale) advancement providing an incentive to participate. The lab sessions involved component assembly and instruction in the operation of the cosmic-ray detectors. We propose to add to this program the AMBER-lite component beginning next summer, including both hardware fabrication and summer lecture and curricular development.

4. QuarkNet Teacher Benefits. The current UH QuarkNet program provides opportunities for teachers' professional development using the Hawaii State Department of Education (HDOE) Professional Development Credits (PDERI) program. Teachers can earn PDERI credits which advance them on their pay scale by showing evidence of the success of their activities with their students. This is done via a portfolio submitted by the teachers to external evaluators in the HDOE. For teachers, QuarkNet provides resources and partnership opportunities that the teachers have no access to otherwise. In addition, the intellectual development opportunities in QuarkNet, with hands-on activities and conceptual material that can be directly transferred to curriculum (lab exercises, science fair projects, class discussion of the latest ideas in particle astrophysics, etc.). The final portfolios that teachers prepare for these credits under QuarkNet provide tangible and quantitative evidence of the effectiveness of the program, and we intend to track the development and impact of our proposed activities through these portfolios, through periodic review and summaries.

G.   Results from Prior NSF Support.

The UH group has not been supported by NSF in the past. The OSU PI has been funded by NSF since 1999 for his role in the Pierre Auger Observatory. He serves as Task Leader for the Surface Detector Electronics, and on the collaboration's Publications and Conference Committees. The group is active both in support of observatory operations and in data analysis. The Auger observatory construction is expected to be completed in 2007, and the first refereed papers are now appearing. The OSU group's NSF support was most recently renewed in 2005.

H.   Broader Impacts at Ohio State.

The science we are involved in is both exciting and accessible, and presents an excellent opportunity for outreach. We are partnering with the high school in Pickerington, Ohio to develop laboratory experiments with simple cosmic ray detectors for their physics program. We recently worked with Pickerington teacher Doug Forrest to secure $11,000 in private support for this effort. Classroom work will begin in early 2007, with the OSU PI and students in attendance. This provides exposure to experimental physics to students at a key phase of their intellectual development, and we hope it will result in more bright students choosing to follow up on their interest in science.

Our work contributes to international understanding in the scientific community. The location of the southern Auger observatory in Argentina has resulted in significant involvement of scientists from less affluent countries where participation in large international projects is less frequent than in more affluent regions. Our activities on the Auger site have afford us the opportunity to interact with many students and scientists from less affluent countries, and created opportunities for exchange of scientific ideas and perspectives. We have found this to be a mutually beneficial exchange; often those who must work with limited resources overcome this seeming obstacle by developing ingenious solutions to problems!

Our group has been and continues to be a welcoming environment for students of all backgrounds. Historically, about 25% of our group has been female. Of seven graduate students currently supported by our group from all sources of support, two are women (Theresa Brandt on CREAM, Kimberly Palladino on ANITA). We continue to encourage broad participation in our work by giving presentations to undergraduate organizations, which often brings our work to the attention of members of underrepresented groups. We have found Latino/a students are particularly intrigued by the fact that our research takes place in Argentina, and we frequently refer to our research when the opportunity presents itself during the course of our teaching activities in order to reach as many students as possible at an early stage in their education.